Hydride transfer catalyzed by xylose isomerase: Mechanism and quantum effects

ARTICLE *in* JOURNAL OF COMPUTATIONAL CHEMISTRY · JANUARY 2003

Impact Factor: 3.59 · DOI: 10.1002/jcc.10154 · Source: PubMed

4 AUTHORS, INCLUDING:

Mireia Garcia-Viloca
Autonomous University of Barcelona
51 PUBLICATIONS **2,330** CITATIONS
SEE PROFILE

Donald Truhlar
University of Minnesota Twin Cities
1,342 PUBLICATIONS **81,416** CITATIONS
SEE PROFILE

Hydride Transfer Catalyzed by Xylose Isomerase: Mechanism and Quantum Effects

MIREIA GARCIA-VILOCA, CRISTÓBAL ALHAMBRA, DONALD G. TRUHLAR, JIALI GAO
Department of Chemistry and Supercomputer Institute, University of Minnesota, 207 Pleasant Street SE, Minneapolis, Minnesota 55455-0431

Received 23 April 2002; Accepted 24 June 2002

Abstract: We have applied molecular dynamics umbrella-sampling simulation and ensemble-averaged variational transition state theory with multidimensional tunneling (EA-VTST/MT) to calculate the reaction rate of xylose-to-xylulose isomerization catalyzed by xylose isomerase in the presence of two Mg^{2+} ions. The calculations include determination of the free energy of activation profile and ensemble averaging in the transmission coefficient. The potential energy function is approximated by a combined QM/MM/SVB method involving PM3 for the quantum mechanical (QM) subsystem, CHARMM22 and TIP3P for the molecular mechanical (MM) environment, and a simple valence bond (SVB) local function of two bond distances for the hydride transfer reaction. The simulation confirms the essential features of a mechanism postulated on the basis of kinetics and X-ray data by Whitlow et al. (Whitlow, M.; Howard, A. J.; Finzel, B. C.; Poulos, T. L.; Winborne, E.; Gilliland, G. L. Proteins 1991, 9, 153) and Ringe, Petsko, and coworkers (Labie, A.; Allen, K.-N.; Petsko, G. A.; Ringe, D. Biochemistry 1994, 33, 5469). This mechanism involves a rate-determining 1,2-hydride shift with prior and post proton transfers. Inclusion of quantum mechanical vibrational energy is important for computing the free energy of activation, and quantum mechanical tunneling effects are essential for computing kinetic isotope effects (KIEs). It is found that 85% of the reaction proceeds by tunneling and 15% by overbarrier events. The computed KIE for the ratio of hydride to deuteride transfer is in good agreement with the experimental results. The molecular dynamics simulations reveal that proton and hydride transfer reactions are assisted by breathing motions of the mobile Mg^{2+} ion in the active site, providing evidence for concerted motion of Mg^{2+} during the hydride transfer step.

 J Comput Chem 24: 177–190, 2003

Key words: xylose isomerase; hydride transfer; tunneling; quantum effects in enzyme catalysis; QM/MM methods

Introduction

Xylose isomerase (XyI) is a bacterial enzyme that catalyzes the interconversion of D-xylose and D-xylulose. It is inducible under conditions where xylose serves as the sole carbon source for growth and metabolism. However, this enzyme displays a broad specificity, accepting the α-anomers of many other pentoses, hexoses, sugar phosphates, and desoxysugars as substrates. Of particular importance is the fact that D-xylose isomerase is able to catalyze the conversion of D-glucose to D-fructose and for this reason is one of the most widely used industrial enzymes. In fact, it is used as the catalyst for an annual production of more than a billion pounds of high-fructose corn syrup, a common food and drink sweetener.[1,2]

XyI is widely distributed in prokaryotes.[2] A multiple alignment of XyI sequences from 18 bacterial sources indicated that the essential structure at the catalytic center is analogous in all the enzymes that were compared. Not surprisingly, given the high degree of sequence homology, the three-dimensional structures of the enzymes from several *Streptomyces* species and from *Arthrobacter* have been found to be very similar, as all of them contain four identical subunits folding into a TIM (triose phosphate isomerase) barrel motif with a well conserved active site located near its center.[1,3] An important aspect of the active site of XyI is the presence of two divalent metal-ion cofactors,[4–7] ligated by a total of seven amino acid side chains (see Fig. 1) that are conserved in all known xylose isomerases. These coordinating residues are congregated to form a highly polar region, and a number of conserved hydrophobic residues lie within 5–8 Å. The residues at the active site are arranged with polar residues on one

Correspondence to: M. Garcia-Viloca; e-mail: garcia@chem.umn.edu

Contract/grant sponsor: National Institutes of Health

Contract/grant sponsor: National Science Foundation; contract/grant number: CHE00-92019

This paper is dedicated to the memory of Professor Peter A. Kollman, whose enthusiasm for science will always be an inspiration.

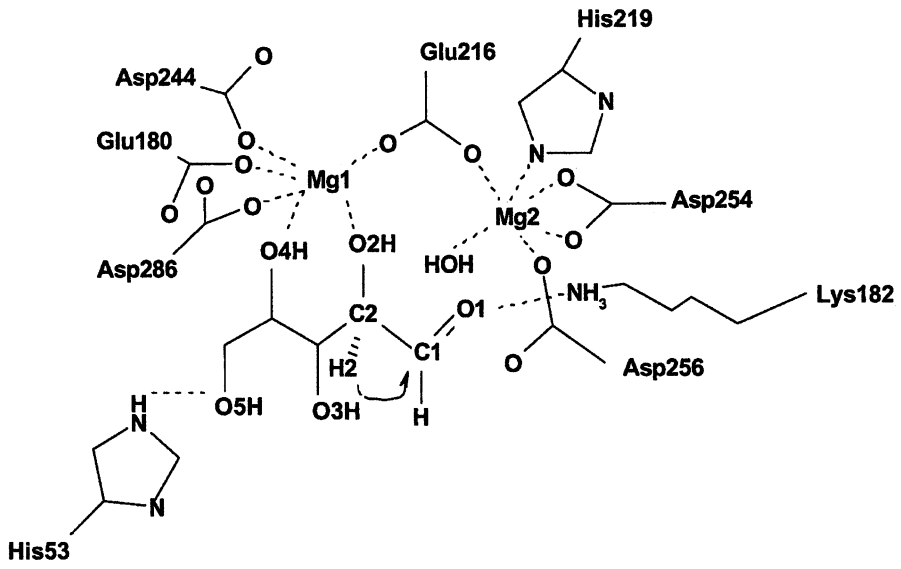

Figure 1. Schematic representation of the active center of xylose isomerase with D-xylose substrate.

side and hydrophobic ones on the other, and this produces an environment of "high hydrophobic contrast" that has been postulated to enhance, respectively, metal and substrate binding in the active site.[8]

The mechanism of XyI, which has been previously investigated both experimentally and computationally,[1] consists of at least three chemical transformations: (1) ring opening, (2) hydrogen transfer between C2 and C1, and (3) ring closure. The aldose-ketose isomerization of the substrate in its open-chain form (step 2) is the rate-limiting step of the overall catalysis.[9] Although the enolization mechanism employed by TIM (leading to an enediolate intermediate) was originally proposed as the pathway of the aldose-ketose isomerization in XyI because of the similarity between their three-dimensional structures, they in fact employ different strategies to accomplish the isomerization of simple sugars.[1,4] The current consensus is that the C2–C1 hydrogen transfer in XyI takes place via an intramolecular hydride shift (with prior and post proton transfers) rather than by an acid-base mechanism. The two main arguments that support this idea, firstly introduced by Farber et al. in 1988,[10] are: (1) that there is no suitable base found in the active site of XyI that could abstract a proton from C2,[4] and (2) that the C2–C1 hydrogen does not exchange with solvent. In the crystal structure, a Trp residue is located in place of a suitable base; it makes a hydrophobic contact with the substrate and excludes solvent from it. Further support was provided by *ab initio* and semiempirical molecular orbital calculations,[11] which led to the conclusion that, in the presence of metal cations in the active site of the enzyme, the hydride transfer pathway has significantly lower activation energy than the proton transfer pathway.

Indication that hydride transfer is the rate-determining step comes from experimentally measured deuterium kinetic isotope effect (KIE) for the overall reaction, in the range of 2.7 to 4.0 for enzymes from different species with glucose substrate at 333 K.[6,12,13] Furthermore, a kinetic study of the enzyme with various metal ions at different pH values showed that a significant barrier appears not for the ring opening, but for the hydride transfer.[9] The same conclusion was reached in the theoretical study of these two steps carried out by Fuxrieter et al.[3] using molecular orbital calculations on three different sized active-site models of XyI.

This article describes a theoretical simulation of the hydride transfer step in XyI and the determination of the primary KIE for this step. For the potential energy surface, we use a combined quantum mechanical/molecular mechanical (QM/MM) method.[14–17] The main aim of this work is to simulate the reaction including quantum effects on the nuclear motion because quantum effects are essential for computing KIEs. With the same objective, Nicoll et al.[18] used a QM/MM potential energy surface to calculate KIEs by variational transition state theory (VTST)[19–21] with small-curvature tunneling (SCT)[22] for a single 42-atom minimum energy path (MEP) in a fixed environment. The room temperature H/D KIE was found to be 6.3, as compared to nontunneling result of 2.4. Adding corrections from a transition state optimized with B3LYP/6-31G changed their computed KIE to 5.8. Our approach differs from theirs in that effects of protein motion, wide-amplitude motion, and flexibility are included in the free energy profile as a function of a reaction progress variable, the transmission coefficient is based on an ensemble of reaction paths corresponding to different protein environments, and the choice of multidimensional tunneling paths is microcanonically optimized for each protein configuration.

Another interesting aspect of the XyI reaction is the requirement of two divalent metal ions such as Mg^{2+}, Co^{2+}, or Mn^{2+}, or a combination of these cations, for maximum activity.[2] Under physicological conditions, it is believed that Mg^{2+} is the preferred metal cofactor for this enzyme.[1] The catalytic activity is inhibited by metals such as Ag^{+}, Hg^{2+}, Cu^{2+}, Zn^{2+}, and Ni^{2+}.[2] In their theoretical study, Fuxreiter et al.[3] compared the effect of different

metals on catalysis, and the activation energies that they obtained clearly showed that Mg^{2+} ions activate, whereas Zn^{2+} ions inhibit the reaction. Ferenczy et al.[23] have confirmed this effect of different metal ions using their fragment self-consistent field method and including a larger polarizable region in their model.

X-ray crystal structures have shown different metal ion positions in substrate and transition state analog complex structures,[24] suggesting that the movements of the Mg^{2+} ions are intimately involved in the enzyme-catalyzed reaction. The density of one of the two magnesium ions (Mg2) in the enzyme-substrate complex is not spherical but has an elliptical shape, in contrast to the structure without substrate. Lavie et al.[8] have interpreted this elliptical density as a shift of Mg2 upon substrate binding from one site, called position 1 (the site occupied in the native structure), to a site closer to Mg1 and the sugar, position 2. The distance between position 1 and position 2 for Mg2 is 1.8 Å. At position 1, Mg2 does not coordinate with the substrate, while at position 2 the ion coordinates with O1 and O2 of the substrate. This result has also been found by other authors in the X-ray crystal structures of XyI from different bacterial strains.[5,7,8,24] Whereas position 2 of Mg2 can only be inferred from the enzyme-substrate complex structure, in the structure with an inhibitor designed to mimic the transition state of the isomerization step this metal ion occupies only this single stable position, that is, the metals are separated by a distance of 4.2 Å, 0.9 Å less than in the apo-enzyme.[24] It is the latter configuration (shorter Mg–Mg separation) that corresponds to the active form of the enzyme for the hydride transfer step in XyI.[24,25] Hu et al.[25] compared different pathways of the metal-induced isomerization step, fixing the metal ion at position 1 or at position 2. Their results indicate that in the enzyme the preferred pathway for the hydride transfer reaction involves Mg2 at position 2. However, the constraint applied on the metal ion positions during their simulation did not allow them to directly assess the movement.

In the present study, starting from a structure suitable for hydride transfer (Mg2 at position 2) we found by QM/MM molecular dynamics simulations that the two magnesium ions move apart as the hydride transfer reaction takes place. Thus, there is a breathing motion of Mg^{2+} ions that mediates the initial proton transfer from O2 of xylose to a hydroxide ion on Mg^{2+} and the subsequent hydride shift reaction in XyI. These dynamic motions of Mg^{2+} ions are included in our calculation.

The simulation method we use in this article is a combination of molecular dynamics simulation with umbrella sampling and ensemble-averaged variational transition state theory with multidimensional tunneling (EA-VTST/MT).[26] This scheme, which has been especially designed for the simulation of enzyme and other condensed-phase reactions, first employs condensed-phase transition state theory[27–29] based on molecular dynamics calculations of a quantized potential of mean force along a distinguished reaction coordinate[30] to identify an ensemble of transition states. Then the theory of rare event sampling[31] is employed to calculate a transmission coefficient by using VTST[19–21] for an embedded cluster[32–35] and semiclassical multidimensional tunneling calculations that include the effect of reaction-path curvature.[22,36,37] The transmission coefficients are then averaged over the transition state ensemble.[26] The incorporation of quantum mechanical effects into enzyme simulation by using QM/MM methods for the potential energy surfaces and semiclassical methods such as EA-VTST/MT for the nuclear dynamics has recently been reviewed.[38,39]

Theory

The present article formulates the rate constant of the reaction catalyzed by XyI by EA-VTST/MT, the formalism of which is presented in detail in a recent article.[26] Transmission coefficients for individual members of the transition state ensemble were evaluated by the static-secondary-zone (SSZ) approximation that has also been presented elsewhere.[26,32–35,40] The potential energy surface (PES) is modeled by a QM/MM method[14–17] that uses the generalized hybrid orbital (GHO) method[17,41] to treat the boundary between the QM and the MM parts of the system (in models where such a boundary is present). In addition we introduce a simple valence bond (SVB)[42] term to improve the accuracy of the PES. Here we summarize the dynamical theory and the procedure, and in the section "Potential Energy Function" we summarize the PES.

Theoretical Framework

For the hydride transfer step in XyI, which is unimolecular, the rate constant at temperature T is written as follows:

$$k^{\text{EA-VTST/MT}}(T) = \gamma(T)k(T) = \gamma(T)\frac{1}{\beta h}e^{-\beta\Delta G^{\neq}(T)} \qquad (1)$$

where $\gamma(T)$ is the overall transmission coefficient, k is the transition state theory rate constant, $\Delta G^{\neq}$ is the transition state theory free energy of activation, h is Planck's constant, $\beta = 1/\tilde{k}T$, and $\tilde{k}$ is Boltzmann's constant. It is clear from eq. (1) that there are two quantities to be computed to estimate the rate constant: (1) the transmission coefficient and (2) the transition state theory free energy of activation; and it is the latter that makes the most sensitive contribution to the rate constant because of the exponential dependence of k on $\Delta G^{\neq}$. The form of eq. (1) suggests that the final rate constant can be obtained in two computational stages.

For comparison to experiment, the rate constant [eq. (1)] is rewritten as

$$k(T) = \frac{1}{\beta h}e^{-\beta\Delta G_{\text{act}}} \qquad (2)$$

where ΔG_{act} is the phenomenological free energy of activation.

In stage 1 of the calculation, the free energy of activation, including the quantum mechanical vibrational free energy, is computed by using a distinguished reaction coordinate to obtain the transition state theory approximation to the quasiclassical rate constant, k.

In stage 2 we correct this transition state theory rate constant with a transmission coefficient, γ, that accounts for (i) classical recrossing (at energies above the effective barrier), (ii) tunneling (at energies below the effective barrier), and (iii) nonclassical diffractive reflection from the barrier top (at energies above the effective barrier). The classical recrossing correction accounts for

the trajectories that recross the transition state theory dividing surface; including only this effect in the transmission coefficient yields the EA-VTST rate constant:

$$k^{\text{EA-VTST}}(T) = \Gamma(T)k(T) \tag{3}$$

where Γ is the ensemble-averaged recrossing coefficient. The rate constant of eq. (3) is called the quasiclassical (QC) rate constant because it includes quantum effects on degrees of freedom orthogonal to the reaction coordinate, but reaction-coordinate motion itself is still treated classically. Then, including (ii) and (iii) yields the final estimate of the rate constant:

$$k^{\text{EA-VTST/MT}} = \gamma(T)k(T) \tag{4}$$

where $\gamma(T)$ is the net transmission coefficient, including dynamical recrossing, multidimensional tunneling, and nonclassical reflection.

In stage 2 the N-atom system is divided into N_1 primary zone atoms and N_2 secondary zone atoms, where $N_2 = N - N_1$, and N is the total number of atoms. For stage 2, only the dynamical effects of the *primary* zone atoms are *explicitly* included in the calculation, but the movement of the secondary zone is partially reintroduced into the reaction coordinate and the transmission coefficient by ensemble averaging, as described below.

Procedures

Stage 1 has two steps:

First, we calculate the classical mechanical (CM) free energy of activation by computing the potential of mean force (PMF) on the distinguished coordinate z, which is defined in the present system as the difference between the breaking bond distance and the making bond distance, that is

$$z = r_{\text{DH}} - r_{\text{AH}} \tag{5}$$

where D is the donor carbon (C2), A is the acceptor carbon (C1), and H is the transferred hydride. The CM PMF can be evaluated by carrying out classical simulations, either molecular dynamics or Monte Carlo simulations, and using umbrella sampling or the free energy perturbation technique. In the present work, the CM PMF is determined by using molecular dynamics for the enzymatic reaction and by using Monte Carlo for the model reaction in water, both with the umbrella-sampling technique[43] to obtain the probability density of configurations, $\rho(T, z)$, with distinguished coordinate z at temperature T. Then

$$W^{\text{CM}}(T, z) = -RT \ln \rho(T, z) + W_0 \tag{6}$$

where W_0 is a normalization constant. In practice, a series of simulations is carried out for a sequence of regions (called windows) along z by adding a restraining or biasing potential to the potential energy function. The biasing potential is the sum of a harmonic term with a minimum at the center of the window and another term that equals minus one times a zero-order estimate of the final $W^{\text{CM}}(T)$. This potential is chosen to allow adequate overlap of the distribution sampled in neighboring windows, and the effect of the biasing potential is removed by statistical analysis to yield the unbiased $\rho(T, z)$. Numerically, the windows are subdivided into bins, and the probability density is collected in bins of width of 0.01 Å, which contributes to a small uncertainty on the value of the reaction coordinate in the computed PMF. The value of z in the bin with the highest $W^{\text{CM}}(T)$ is called z^*_{CM}. The CM transition state theory free energy of activation is obtained as

$$\Delta G^{\text{TST/CM}}(T) = W^{\text{CM}}(T, z^*_{\text{CM}}) - [W^{\text{CM}}(T, z_R) + G^{\text{CM}}_{R,F}(T)] \tag{7}$$

where $G^{\text{CM}}_{R,F}(T)$ is the classical free energy of the internal degree of freedom that correlates with the distinguished coordinate z, because it is not included in the CM PMF. We note that the derivation of eq. (7) assumes a rectilinear z, and the choice of z in eq. (5) is close enough to rectilinear that the correction for the curvilinear nature of z is expected to be small (less than RT). We also note that eq. (7) assumes separability of z from the other coordinates in the reactant region, and again the error due to that assumption (at least for the present system) is expected to be small; the procedure we actually use (a reference is given below) is better than assuming global separability.

Second, we carry out instantaneous normal mode analysis for the atoms of the primary subsystem (for many configurations in each of several bins of the umbrella-sampling step) to obtain the average generalized normal mode frequencies.[30] These are used to compute a quantum mechanical vibrational free energy correction $\Delta W_{\text{vib}}(T, z)$, which is the difference between the quantal vibrational free energy and the classical vibrational free energy of the $3N_1 - 7$ highest vibrational modes, all of them orthogonal to the distinguished coordinate, because it has been projected out of the Hessian with a projector operator.[30] The values of $\Delta W_{\text{vib}}(T, z)$ at the centers of the bins in which it is directly computed are interpolated to the centers of other bins by local cubic fits. This correction is added to the CM PMF to produce a QC PMF:

$$W^{\text{QC}}(T, z) = W^{\text{CM}}(T, z) + \Delta W_{\text{vib}}(T, z) \tag{8}$$

Then, a QC free energy of activation is the difference of the QC PMF at the transition state (z^*), which is the value of z where $W^{\text{QC}}(T, z)$ has a maximum, and at the reactants (z_R), minus the quantized value of $G^{\text{CM}}_{R,F}(T)$. This is the quantity already mentioned in eq. (1):

$$\Delta G^*(T) = W^{\text{QC}}(T, z^*) - \lfloor W^{\text{QC}}(T, z_R) + G^{\text{QC}}_{R,F}(T) \rfloor \tag{9}$$

where for the reactant (R) state we have to add the quantized free energy, $G^{\text{QC}}_{R,F}$, of the mode that correlates with the distinguished coordinate z, because, as mentioned above, it is not included in the PMF. A procedure for estimating $G_{R,F}$ has been presented previously[26] and was used here.

Stage 2 has the objective of computing the transmission coefficient, $\gamma(T)$, which is the product of two factors, κ and Γ, and contains the dynamical effects that are not already included in the TST result (recall that a TST rate is equivalent to a one-way flux through a hypersurface with $z = z^*$[19,20]). The first factor, which is the quasiclassical transmission factor, Γ, corrects the rate con-

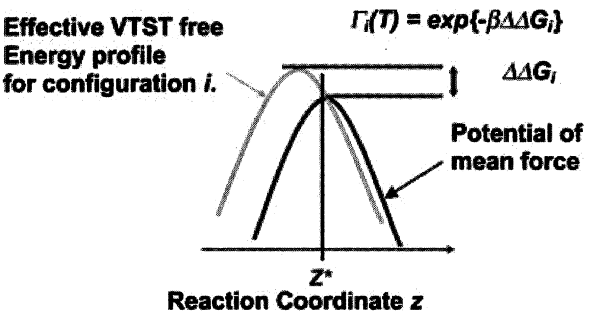

Figure 2. Schematic explanation of the quasiclassical transmission coefficient calculated at stage 2. [Color figure can be viewed in the online issue, which is available at www.interscience.wiley.com.]

stant for classical dynamical recrossing.[26,31] The second factor, κ, is the semiclassical transmission coefficient that accounts mainly for tunneling, that is, the quantum effect on the reaction coordinate, which is missing in the calculation of the QC rate constant.

In stage 2, the calculations are carried out using an equilibrium distribution of secondary-zone configurations, labeled $i = 1, 2, \ldots, I$, in the bin corresponding to $z = z^*$, where, as stated above, z^* is the location of the stage-1 variational transition state (as optimized at step 2 of stage 1). For each transition state configuration i, we freeze the secondary-zone atoms and optimize the saddle point structures of the primary-zone atoms by treating them as a cluster embedded in the potential field of the fixed secondary-zone atoms. Then, an isoinertial MEP is calculated through the $3N_1$-dimensional primary zone by the embedded cluster method.[32–35] The individual paths obtained for the different configurations i are effective PMFs that describe the dynamics of the primary-zone atoms under the effective potential of the rest of the system for the various configurations. Individual semiclassical transmission coefficients κ_i can be calculated by employing methods fully described in previous work.[20,22,26,37] And for each configuration the Γ_i factor is a function of the difference in free energy between its maximum in the MEP calculation and its value at the point for which z equals to z^* (see Fig. 2). The product of these two factors, κ_i and Γ_i, gives the net transmission coefficient for configuration i.

$$\gamma_i = \kappa_i \Gamma_i \tag{10}$$

Averaging just the recrossing correction over I secondary-zone configurations gives the most complete QC rate constant in eq. (3), where $\Gamma(T) = \langle \Gamma_i \rangle$. Averaging the total transmission coefficient over I secondary-zone configurations gives the final stage-2 rate constant in eq. (4), where $\gamma(T) = \langle \gamma_i \rangle$.

In the present work we have not applied the so-called equilibrium secondary zone approximation[26] that introduces the change in free energy of the secondary zone system along the primary zone reaction coordinate. The result of including this free energy change on the rate constant and KIEs in the hydride transfer reaction catalyzed by liver alcohol dehydrogenase showed that, for that relatively rigid active site, inclusion of this effect does not significantly change the results.[26]

Details of the Calculations

Model

The starting point of the simulation was the X-ray structure of XyI with D-glucose bound in the active site, resolved by Lavie et al.[8] (code number 1XYB in the Protein Data Bank, PDB). This structure contains the Cartesian coordinates for the enzyme atoms of the dimer contained in the crystallographic asymmetric unit, with one D-glucose molecule and two Mg^{2+} ions per active site, with one active site for each monomer, and 481 crystallographic waters in the dimer. There are 386 residues per monomer, and the active site of each monomer in the dimer contains residues from the other monomer.

Calculations[8] of the solvent-accessible surfaces of possible dimers suggest that the tetramer of 222 symmetry is the active form of this XyI. Following the analysis of Lavie et al.,[8] we generated the Cartesian coordinates of the atoms of the second dimer by applying a twofold rotation in the space group $P2_12_12$. Although there is no apparent cooperativity among the four active sites, it is still necessary to construct the tetrameric structure because residues from different subunits can be present in the simulation system. We substituted the D-glucose molecule found at each active site of the tetramer with a D-xylose molecule. In addition, a 24 Å sphere of equilibrated waters was centered around the reactive center, which is taken as the geometric center of atoms O2–C2–C1–O1 in one of the monomers (which is chosen at random because they are all the same). Water molecules at a distance less than 2.5 Å from any protein atom or crystallographic water were removed. The final system contained 25,317 atoms. This includes 76 substrate atoms (19 atoms in each of the four substrates), 1461 atoms in 487 water molecules, and 23,780 atoms in the enzyme, including the eight Mg^{2+} ions (two in each monomer).

Stochastic boundary molecular dynamics (SBMD) was used to treat the system,[44] in which the dynamics region consists of all water and amino acids residues that have any atoms within 20 Å from the center, and it is surrounded by a buffer region. The buffer region contains waters and amino acids that have any atoms within 24 Å of the center not belonging to the dynamics region. All other atoms were assigned to the reservoir (or outside) region and were kept frozen in the molecular dynamics calculations. The dynamics region was treated by unconstrained Hamiltonian dynamics, whereas the dynamics in the buffer region was propagated by Langevin dynamics, which allows energy transfer between the reservoir and dynamics regions.[44] We used an integration time step of 1 fs in all calculations along with a nonbonded cutoff of 13 Å based on the center-of-mass separation between interacting groups. Protein atoms were assigned to one or another region according to a reference structure at the start of the simulation and retained their labels throughout the simulation, whereas water molecules were allowed to switch between regions. A deformable boundary potential[44] was imposed on water molecules at the buffer/reservoir interface to represent the effect of bulk solvent outside this boundary. In all simulations the three internuclear distances of the water molecules, except for one water in the active site at the origin, and all chemical bonds of the protein involving hydrogen atoms, were frozen by the SHAKE algorithm.

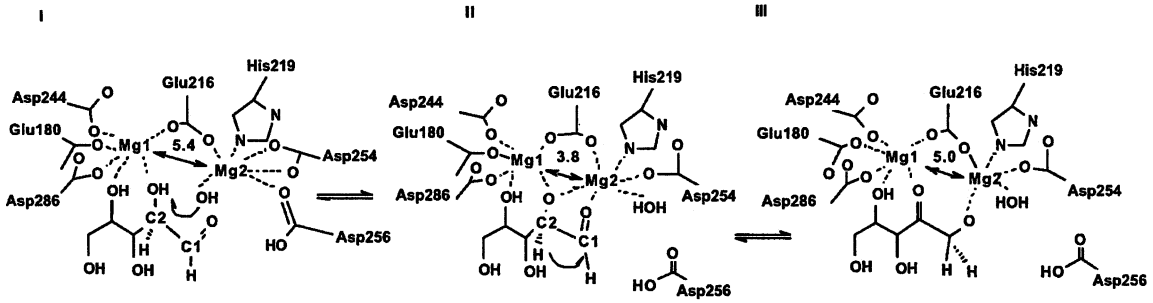

Figure 3. Proposed mechanism for xylose isomerase reaction. The distances between Mg^{2+} ions correspond to the X-ray values determined by Ringe et al.[7,8,24]

The total charge of the system was −24 (−6 for each monomer). In one monomer there were 52 positively charged residues (Arg, Lys, and His), 61 negatively charged residues (Asp and Glu), 2 Mg^{2+} ions, and one negative charge from D-xylose substrate deprotonated (in the three MM active sites) or from the OH^- ligand of Mg2 at the QM active site. The total charge within a sphere of 10 Å around the D-xylose substrate (at the active center used to simulate the enzymatic reaction) was −1 (+2 Arg + 3 Lys + 3 His − 7 Asp − 5 Glu + 2 Mg^{2+} − 1 OH^-). The total charge in the zone between 10 and 20 Å from the D-xylose substrate was +12(+22 Arg + 10 Lys + 7 His − 16 Asp − 11 Glu).

The configuration of the active site in the X-ray structure corresponds to the state prior to the proton transfer that precedes the hydride transfer; this configuration is represented as complex **I** in Figure 3. In order to study the hydride transfer reaction schematically represented by the conversion between complexes **II** and **III** in Figure 3, it is necessary to generate a structure that is a good starting point for this reaction step. To accomplish this, we evolved a structure from **I** by a sequence of operations (see below).

The starting structure of the reactant complex for the hydride transfer step was constructed according to the mechanism shown in Figure 3 that was based on that proposed by Whitlow et al.[5] and included the structural information of ref. 8. In this mechanism, the 2-hydroxy proton of the substrate is first transferred to a hydroxide ion that is ligated to Mg2, which leads to the replacement of one of the bidentate interactions between Mg2 and Asp254 with an interaction with the 2-alkoxide anion. Concomitantly, Mg2 migrates about 1 Å towards Mg1 to resume the second position described above: this is the active configuration for the hydride transfer step (complex **II** in Fig. 3), and the carbonyl group of the substrate becomes a ligand to Mg2, replacing the neutral Asp256 (Asp256 is protonated by abstracting a proton from the water molecule, which then becomes the hydroxide shown in structure **I** and the base that abstracts a proton from the 2-hydroxy group of the xylose). Notice that this structural variation does not change the overall charge on all ligands coordinating Mg2.

From the X-ray structure with D-glucose bound, where the configuration of the residues in the active site corresponds to complex **I** in Figure 3, we simulated the proton transfer and the Mg1–Mg2 approaching using the umbrella-sampling technique. First this required some choices, which we made as follows:

1. In the X-ray structure there are two sets of coordinates for Mg2 in each active site; the Cartesian coordinates that correspond to position 1 were chosen, and the O2 atom of the xylose molecule was protonated in the active site that we used to simulate the reaction. (In the other three active sites, we chose the Cartesian coordinates that correspond to position 2, and we used a deprotonated xylose molecule.)
2. All histidine residues were protonated in the present calculation, with the exception of His219, to simulate a pH of approximately 6 and to decrease the negative charge in the system.
3. In addition, we also protonated Asp256 in the four active sites.

Starting with this structure, we used molecular dynamics with umbrella sampling to evolve structure **I** along a reaction coordinate defined as the distance of the proton from the donor minus the distance of the proton from the acceptor. After this proton transfer was accomplished, the Mg–Mg distance was still large, so we evolved the system along another reaction coordinate defined as the Mg–Mg distance. Because of the very short time scale that can be accessed in molecular dynamics simulations, the final structure of this step still involved the same coordination pattern as in Figure 1. The Mg2–O1 distance was still large because the dihedral angle O1–C1–C2–O2 was far from zero. To prepare a starting structure for the hydride shift (Fig. 3), the carboxylate group of Asp254 was rotated around the C_α—C_β bond to leave only one oxygen coordinating to Mg2, and we replaced the Asp 256 coordination with the O1 atom of the substrate, by rotating the O1–C1–C2–O2 dihedral angle from 90° to 5° and moving the carboxyl group of Asp256 away from Mg2. Again, there is no net change in the total charge of the Mg2 coordination sphere. The resulting structure was minimized in a 24 Å sphere around the active center for 20 steps to remove possible close contacts using the ABNR method in CHARMM.[45] This yielded a structure suitable for use as a starting point for simulating the hydride transfer. This structure is provided in Supporting Information in Protein Data Base format.

Potential Energy Function

The PES was calculated by a mixed QM/MM method[14,17] augmented by an SVB[42] term. For the QM/MM calculations, the system was partitioned into N_{QM} quantum mechanical atoms and N_{MM} classical mechanical atoms.

For this study, we used two models that contain the same total number of atoms but differ in the partition. Model 1 was used primarily to develop an initial structure for the rate-determining step and to gain additional insight into the quantum mechanical character of the Mg^{2+} cofactor, and included both Mg^{2+} atoms together with the side chains of all their ligands in complex **I** (Fig. 3) in the QM representation. Model 2, which was used for the final PMF calculations, contained 19 QM atoms that correspond to the xylose molecule with O2 deprotonated, and there were no boundary atoms or generalized hybrid orbitals.

In model 1, N_{QM} equals 79, the MM systems include seven boundary atoms that are treated partly by MM and partly with the GHO[17,41] method. The boundary atoms are the C_α atoms of the backbone for the His and four Asp residues and the C_β atoms of the sidechain for the two Glu residues. The total number of atoms and the charges in the system are the same in the two models, but the atoms contained in the reactant/buffer/reservoir regions are slightly different because the reference structure is different, although the reactant region radius (20 Å) and buffer region outer radius (24 Å) are the same. The larger QM atom model was used to generate the initial structure to simulate the hydride transfer with both models, by running the PMFs for the proton transfer and the Mg–Mg approach. The reference structure for this model was the one obtained after building the model from the X-ray structure with replacement of glucose by xylose in the active site, a definition of the origin of the coordinate system as the center of the active center, and assignment of appropriate protonation states of titratable residues. Then the QM part of the system was minimized for 20 steps using the Adopted Basis Newton-Raphson method (ABNR) of CHARMM,[45] after which spheres of waters were added successively until all the spaces that were large enough to hold waters were filled. After this, all the waters and a 15 Å sphere around the center were minimized for 100 and 20 steps, respectively, with the ABNR method. Then, MD simulations were carried out at 150 K for 5 ps for water molecules within the 24 Å sphere from the reactive center. In this calculation all protein atoms were kept rigid. We then repeated this process a second time. The total number of additional waters added was 263. In addition, the tetramer had 962 crystallographic waters, but we deleted 738 of these waters that were outside the 24 Å sphere from the origin. The resulting structure was the reference structure for model 1 with 79 QM atoms. The total number of atoms for this model in the dynamics and buffer region was 7999, and in the reservoir region it was 17,318.

In the 19-QM-atom model (model 2), which is the final model used to calculate the KIEs (with model 1 we did only one dynamics calculations for the hydride transfer step, taking one secondary zone configuration), the dynamics region contained 4777 atoms from all four monomers, but most of these atoms were in the one monomer singled out as the reactive monomer. The dynamics region included one xylose molecule (19 atoms), two Mg^{2+} ions, and 3973 protein atoms, while the buffer region contained 2507 protein atoms. There were a total of 1458 water molecules in the reaction zone, and the reservoir region contained 17,358 atoms.

For both models the QM subsystem was described by the PM3 semiempirical model[46] with specific reaction parameters for Mg^{2+} ions (see below), whereas the MM system was represented by using the CHARMM22 all-atom MM force field,[47] and the water molecules were modeled by the TIP3P MM force field.[48]

Table 1. Computed Mulliken Population Charges and Average Geometrical Parameters Obtained with Model 2 for the Substrate Atoms that Participate in the Hydride Transfer Step in the Active Center of XyI.[a]

	Reactant state	Transition state	Product state
Charges			
O1	−0.59	−0.84	−1.06
C1	0.39	0.33	0.25
O2	−1.13	−0.92	−0.55
C2	0.10	0.24	0.34
H2	0.11	0.00	0.02
Geometrical parameters			
O1–C1	1.23	1.28	1.34
O2–C2	1.38	1.31	1.22
O2–C2–C1–O1	−2.03	6.14	11.24

[a]Charges are given in atomic units, distances in angstroms, and angles in degrees. Model-2 calculations (19 QM atoms) are based on PM3 for the QM subsystem, and they include an SVB term. Geometrical parameters are averaged over 300 configurations.

Classical molecular dynamics simulations for the 19-QM-atom model of the substrate-enzyme system yielded a barrier of 25.6 kcal/mol. Table 1 shows the evolution of the geometry and the charges on the substrate atoms in the active site for the reactant, transition state, and product, and Table 2 summarizes the distances obtained between Mg^{2+} ions and their ligands in the active site. There is a general agreement with the experimental results that validates the model.

Model 1 of the active site (with 79 QM atoms) allows charge transfer between the Mg atoms and the ligands and therefore would be in principle a better representation of the reaction process if PM3 parameters for Mg^{2+} were accurate enough. However, following the procedure used to compute the free energy of activation with model 2, we obtained a barrier that is 13 kcal/mol higher than that in model 2. In addition, the distances between the Mg^{2+} ions and their ligands were too short at the reactant, transition state, and product structures in model 1 in comparison with distances from *ab initio* calculations on model complexes and from X-ray crystal structure in the complex of XyI with D-glucose. Further, several theoretical studies on model compounds have indicated that the amount of charge transfer to the catalytic metal is crucial for determining the activation energy in the reaction catalyzed by XyI.[3,23,49] It was found that there is little charge transfer for activating ions such as Mg^{2+}, Mn^{2+}, and Co^{2+}, whereas the amount of charge transfer to the metal is large for deactivating Cu^{2+} and Zn^{2+} ions. We tested the performance of the PM3 semiempirical model on two systems: $Mg(H_2O)^{2+}$ and $Mg(OOCCH_3)^+$. In agreement with the results obtained by Fuxreiter et al.,[3] charge transfer is significantly greater using PM3 than that at the MP2 level. Thus, it appears that the higher barrier obtained using model 1 is due to an overestimation of charge transfer from the O2 oxygen to Mg^{2+}, which inhibits the formation of a carbonyl π bond, and in turn, the hydride transfer reaction.

Table 2. Average Interatomic Distances for Selected Residues in the Active Site of XyI Obtained with Model-2 (19 QM Atoms) and Results from X-Ray Crystallographic Structures.[a]

	Reactant state	Transition state	Product state	Exp1[b]	Exp2[c]	Exp3[d]
Interactions with Mg1						
Glu180 OE	1.92	1.91	1.89	2.1	2.4	2.2
Glu216 OE	1.87	1.88	1.87	2.2	2.4	2.1
Asp244 OD	3.30	2.03	1.98	2.2	2.4	2.1
Asp286 OD	1.92	1.95	1.95	2.2	2.4	2.1
Xylose O2	1.98	2.09	2.10	2.3	2.4	2.4
Xylose O4	2.14	2.15	2.30	2.3	2.4	2.3
Interactions with Mg2						
Glu216 OE	1.93	1.94	1.94	2.7	2.4	2.1
His219 NE2	2.14	2.14	2.12	2.1	2.5	2.5
Asp254 OD	1.95	1.96	1.99	3.1	—	2.7
H_2O	2.03	2.03	2.04	1.9	2.5	2.1
Xylose O1	2.08	1.95	1.89	2.6	2.5	2.6
Xylose O2	2.01	2.10	3.46	2.4	2.4	3.2
H_2O'[e]	4.05	3.85	2.12	—	2.5	—
Substrate − protein hydrogen bonds						
Xylose O1 − Lys182	1.97[f]	1.84[f]	2.65[f]	3.1[g]	2.7[g]	3.0[g]
Xylose O5 − His53	2.57[f]	2.84[f]	2.08[f]	2.9[g]	2.8[g]	3.2[g]

[a]Distances are given in angstroms and the root-mean-square fluctuations are typically ±0.1 Å. The averages are done over 300 configurations for each state.
[b]Ref. 5. Complex between xylose isomerase and xylose.
[c]Ref. 24. Complex between xylose isomerase and a transition state analog.
[d]Ref. 6b. Complex between xylose isomerase and xylose.
[e]See section "Breathing Motions of the Metal Ions in the Active Site".
[f]Distance between hydrogen and the acceptor atoms.
[g]Distance between the donor and acceptor atoms.

Hutter et al.[50] recently developed a set of Mg^{2+} parameters for use in the AM1 model. Using this parameter set along with the AM1 model, we found that the Mulliken charge distribution and the optimized Mg-ligand distances are in reasonable accord with *ab initio* MP2/6-31G(d) results for the two model compounds noted above; however, the computed interaction energies are weaker. As a result, the interaction between Mg1 and the O4 atom of xylose was lost during molecular dynamics simulation of the reactant complex.

Combining the good features of the PM3 and AM1 parameters for Mg^{2+}, we found that the best results in semiempirical calculations were obtained by using the PM3 model for all atoms except Mg^{2+}, while the Mg^{2+} ion was described by the AM1-type parameters with U_{ss} and U_{pp} values reduced by 10%. We do not consider this as an arbitrary mixing of AM1 and PM3 parameters, rather, we consider the modified Mg model as a PM3-specific reaction parameter (SRP)[51] set. Table 3 shows the amount of charge transfer between Mg^{2+} ions and the substrate in the active site of model 1. In spite of the difference between the absolute value of the charges on the atoms for the two models and the difference in charge transfer from xylose to the magnesium ions, the charge evolution on the substrate along the reaction follows the same general trends. Overall, the agreement between the two models suggests that the interaction between Mg^{2+} ions and their ligands in the active site of XyI can be adequately described by a simple electrostatic model for the metal ions without explicitly treating them in the QM subsystem. This allowed us to use the computationally less expensive 19-QM-atoms model (model 2) in the free energy calculations described below.

Table 3. Computed Mulliken Population Charges for the 79-QM Atom Model (Model-1).[a]

Charges	Reactant state	Transition state	Product state
O1	−0.30	−0.51	−0.67
C1	0.26	0.30	0.16
O2	−0.51	−0.39	−0.21
C2	0.04	0.17	0.23
H2	0.09	−0.09	0.00
Mg1	0.76	0.78	0.81
Mg2	0.72	0.73	0.75

[a]Charges are given in atomic units for the substrate atoms that participate in the hydride transfer step in the active site of XyI. Model-1 calculations are based on PM3-SRP for the QM subsystem and do not include the SVB term.

In order to obtain an even more accurate PES, we added a SVB term[42] to the QM/MM potential energy function for the model 2 calculations. This approach is based on the assumption that the shape of the PES for the hydride transfer reaction is reasonably represented by the PM3 model. This is a valid assumption because the energy correction term changes the energies at two critical points by only a few kilocalories per mole. The SVB term is a combination of two Morse potentials, which depend on the bond distances of the breaking and making bonds, respectively, and a constant term that couples them. In particular, the final model 2 PES is

$$V = V_{\text{QM/MM}} + V_{\text{SVB}} \tag{11}$$

where the first term is the QM/MM potential based on PM3, the CHARMM22 protein force field, and TIP3P, and the second term is

$$V_{\text{SVB}} = \frac{1}{2}[M_1(r_{\text{DH}}) + M_2(r_{\text{AH}}) - \sqrt{(M_2(r_{\text{AH}}) - M_1(r_{\text{DH}}))^2 + 4V_{12}^2}] \tag{12}$$

where $M_i(r_i)$ is a Morse curve given by

$$M_i(r_i) = D_i[e^{-2\alpha_i(r_i - r_i^0)} - 2e^{-\alpha_i(r_i - r_i^0)}] \tag{13}$$

and V_{12} is a coupling element. Although one might take V_{12} to be a function of the donor-acceptor distance or other geometrical variables in the general case, in the present work it was taken as a constant for simplicity. Therefore there are seven parameters. As discussed in more detail below, we adjusted the parameters to match the *ab initio* results for a model hydride transfer reaction, and they were further refined on the basis of the experimental k_{cat} for the enzymatic reaction. The resulting potential is intended to provide reasonable results close to the critical points on the reaction path, and it is not claimed to be quantitatively accurate for global features of the potential surface. The SVB potential was used for the sole purpose of correcting quantitative errors from semiempirical calculations, assuming that the shape and curvature of the latter model are adequate.

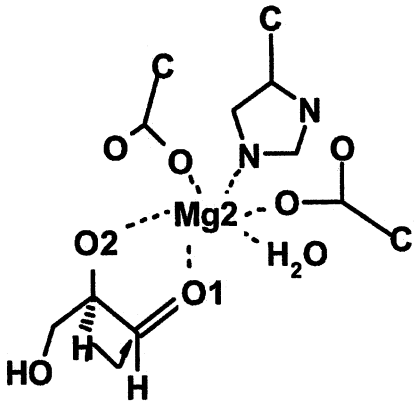

Figure 4. Schematic representation of the primary zone atoms used for the dynamics calculations.

Dynamics Calculations

A SBMD simulation[44] along with umbrella sampling of the reactants of the hydride transfer reaction with O2 deprotonated at 298.15 K was performed to determine the PMF along the reaction coordinate z, defined as in eq. (5). Starting from the structure for the reactants that was equilibrated by a 50-ps simulation, we used 15 consecutive windows, each of which spanned a range of 0.1 to 0.3 Å to reach the product state. For each window the starting structure and velocities were taken from the last structure of the previous window. Then, for each window, the system was further equilibrated for 5 ps, and the probability density of configurations was collected for 25 ps.

For the following calculations we defined the atoms that are represented in Figure 4 as the primary zone atoms (thus $N_1 = 32$ in the notation of the "Theoretical Framework" section), and we used the CHARMMRATE[52] module of CHARMM,[45] based on an interface of CHARMM and POLYRATE.[53] Different sizes of the primary zone atoms were tested and we chose the smallest system, 32 atoms, that allows the relative distance between the magnesium ions in the active center to change, giving reasonable energetic results. The quantum mechanical vibrational energy correction was added to the CM PMF by carrying out normal mode analysis for 100 configurations of the product and reactant windows and 192 configurations from two windows at the transition state zone of the CM PMF. The same configurations were used for both hydride and deuteride shifts. The Hessian was determined numerically by a central difference scheme with a step size of 0.01 bohr, and the generalized normal modes were calculated in rectilinear coordinates. When calculating generalized normal mode frequencies, the reaction coordinate was projected out of the Hessian, as mentioned in the "Procedures" section and as described in refs. 26 and 30. The calculated frequencies for the various configurations were averaged over all the configurations that belong to a given bin of width 0.01 Å, and the correction of eq. (8) was calculated as a function of the averaged frequencies. Figure 5 shows the quantum mechanical vibrational energy correction for the hydride transfer case as a function of the reaction coordinate. The discrete values in individual bins were fitted to a cubic-polynomial function as shown in Figure 5. The same procedure was used for the deuteride transfer.

From the classical simulation, we chose five bath configurations within the interval $z^* \pm 0.06$, where z^* is the value of the reaction coordinate at the maximum of the quasiclassical PMF, to perform the stage 2 VTST calculations. For KIE calculations we used the same configurations for the deuteride case as for the hydride case. Geometry optimizations of the primary zone reactant and product species were performed using the BFGS method, while the saddle point geometry was obtained using the Newton-Raphson method with Brent line minimization[54] with the gradient converged to 10^{-7} atomic units. The reaction path was traced using the Euler steepest descent method[55] in mass-scaled coordinates with a reduced mass of 1 amu and a step size of 0.002 bohr.

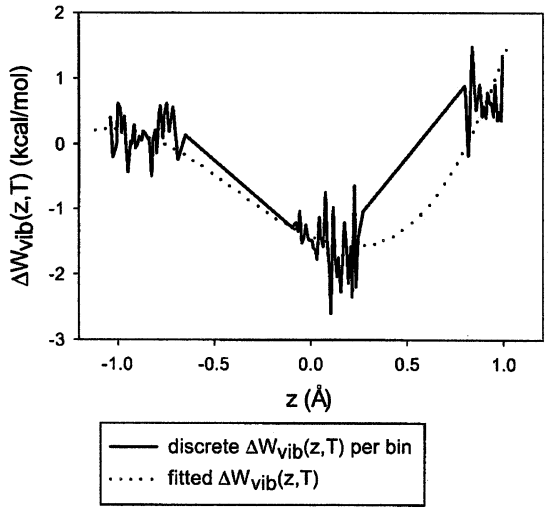

Figure 5. Quantum vibrational free energy correction along the CM PMF for the hydride transfer reaction.

The MT transmission coefficient, $\kappa(T)$, was microcanonically optimized between the SCT value calculated by using the centrifugal-dominant small-curvature semiclassical adiabatic algorithm,[22] and the large-curvature tunneling (LCT) value was determined with the version-4 algorithm.[37]

Calculations on Gas-Phase System and in Aqueous Reaction

In order to validate the PM3 method we also carried out gas-phase calculations on the model system shown in Figure 6, and to explore the interactions underlying enzymatic catalysis, we also carried out simulations of this model reaction in aqueous solution without the enzyme present. The gas-phase calculations involved Møller-Plesset second-order perturbation theory (MP2)[56] with the 6-31 + G(d)[57] basis set. We used the model represented in Figure 6 with the addition of an MM Mg^{2+} ion between the oxygen atoms to study the hydride transfer reaction in aqueous solution. For the model hydride transfer reaction in water, Monte Carlo statistical mechanical simulations were performed using the QM/MM (PM3/TIP3P) potential and the MCQUM program.[58] In the latter calculation, only atoms of the aldehyde/ketone molecule were represented in the QM region. We note that it would be meaningless to directly compare the experimental rate constants of the hydride transfer reactions in water and in XyI because they would proceed via different mechanisms. However, it is possible to do so computationally and the purpose of this comparison is to examine the different features of the enzyme reaction in water as if it were taking place following the same mechanism.

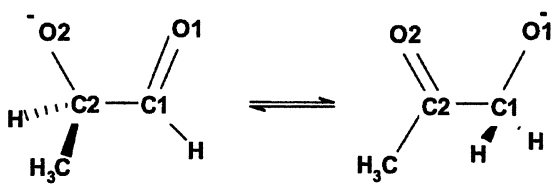

Figure 6. Small model for the hydride transfer step.

Results and Discussion

Classical Potential of Mean Force

The performance of the PM3 method for the quantum mechanical subsystem of the present reaction was investigated by comparison with results from MP2/6-31 + G(d) calculations for the gas-phase process in Figure 6. The energy barrier between the reactant and the transition state is 15.0 kcal/mol at the MP2 level, and the reaction is exoergic by 0.2 kcal/mol. On the other hand, PM3 calculations overestimate the barrier by 4.1 kcal/mol and the exoergicity by 3.5 kcal/mol. Zheng et al.[11] used a similar model to examine the mechanism of aldehyde/ketone isomerization, but they included a Mg^{2+} ion between the oxygen atoms. Their PM3 results indicate that the presence of a Mg^{2+} ion increases the barrier height by 4.7 kcal/mol to a value of 25.5 kcal/mol.

Next we performed calculations on the enzymatic reaction, with 19 QM atoms treated by PM3 and without an SVB term, and we obtained a preliminary CM free energy barrier of 30 kcal/mol, which is much greater than the experimental values of 16–20 kcal/mol from two sets of studies.[6,13] To achieve a better agreement, we included an empirical SVB term in the QM/MM potential, which lowered the free energy barrier by 5 kcal/mol and decreased the exoergicity by about the same amount. The SVB term is included in all calculations employing model 2. The final parameters are listed in Table 4. The results of the Monte Carlo simulation for the hydride transfer step in aqueous solution are summarized in Table 5. The average partial atomic charge on the C1 atom is more positive than that on the C2 atom in the reactant state, which provides an attractive force to facilitate the hydride transfer to the terminal group. The calculated free energy barrier is 22 kcal/mol in water, which is higher than the PM3 energy barrier in gas phase calculations (19.1 kcal/mol). It is interesting to compare the results for the enzymatic reaction and for the reaction in water, which are obtained using the same model by treating the substrate quantum mechanically and the environment, including the Mg^{2+} ions, classically. Tables 1 and 5 show that the average atomic charges of the substrate along the reaction path are similar for the reaction in water and in the enzyme. Note that in all 10 cases (five atoms proceeding from reactants to transition state and

Table 4. Parameters for the Simple Valence Bond (SVB) Potential for the Hydride Transfer Reaction in Xylose Isomerase.

	D_i (kcal/mol)	α_i (Å)	r_i^0 (Å)	V_{12} (kcal/mol)
C2–H	108.3	0.6	1.15	
C1–H	97.5	1.2	1.14	
C2–C1				35.0

Table 5. Average Mulliken Population Charges and Geometrical Parameters for the Model System[a] in Aqueous Solution.

	Reactant state	Transition state	Product state
Charges			
O1	−0.81	−0.99	−1.12
C1	0.47	0.31	0.19
O2	−1.12	−0.96	−0.81
C2	0.18	0.34	0.43
H2	0.10	0.01	0.08
Geometrical parameters			
Mg–O1	1.83	1.83	1.83
Mg–O2	1.84	1.89	1.89
O1–C1	1.24	1.34	1.36
O2–C2	1.39	1.35	1.28
O2–C2–C1–O1	3.68	−1.52	−8.2

[a]Figure 6 with the addition of one Mg^{2+}.
Charges are given in atomic units, distances in angstroms, and angles in degrees.

then proceeding from transition state to product), the direction (sign) of the change of the charge is the same in the enzyme and in aqueous solution, although there are quantitative differences in the magnitude of the changes in the charges.

Breathing Motions of the Metal Ions in the Active Site

Figure 7 depicts the variation in the average distance between the two Mg^{2+} ions as a function of the hydride transfer reaction coordinate. The average Mg1–Mg2 distance at the reactant is in good agreement with that for the second magnesium position found in the structure of the complex with D-glucose.[8] This is the reactive position for the hydride transfer step, where Mg2 is closer

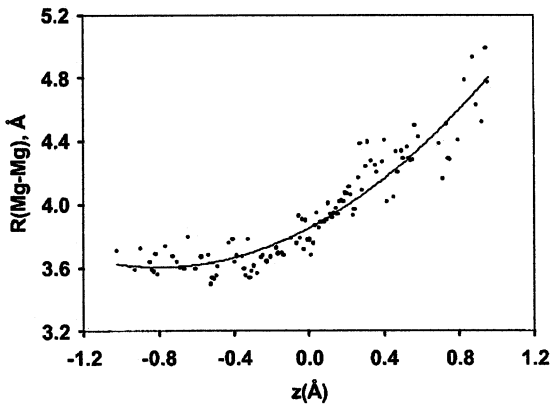

Figure 7. Computed Mg–Mg distance as a function of the hydride transfer reaction coordinate for conversion of xylose to xylulose in xylose isomerase. The magnesium separation is accompanied by the migration of the hydride from the C2 carbon to the C1 position, resulting in a 1-alkoxide anion that favors strong binding with Mg2.

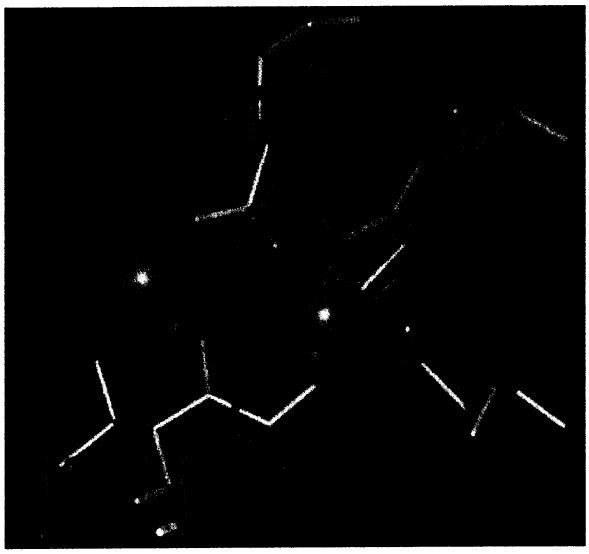

Figure 8. Superimposition of the structures corresponding to the reactant (colored) and product (yellow) states in the active center of XyI. These structures are the last configuration from the window closest to these states during the umbrella-sampling simulation.

to Mg1. As the hydride transfer reaction proceeds, the magnesium distance increases by more than 1 Å, and a superimposition of the reactant and the product structures is depicted in Figure 8. The average Mg1–Mg2 distance at the transition state has a value that is very similar to the distance (4.2 Å) in the X-ray structure of the complex with a transition state analog.[24] In the reactant state for the hydride transfer, the substrate 2-alkoxide anion is ligated to both magnesium ions,[24] which, along with Glu216, are primarily responsible for keeping the two Mg ions in close proximity. As the product is formed, which transforms the O2 alkoxide anion to a neutral carbonyl group, the binding force is much weaker between the O2 oxygen and the two Mg^{2+} ions (Fig. 3). Thus, the two Mg ions move to a greater separation during the simulation, that is, in an opposite direction to the movement proposed for the previous proton transfer step.

At the product state the interaction between O2 and Mg2 has been replaced by a new interaction between the metal ion and a second water molecule (labeled as H_2O' in Table 2) that has entered in the active site. A second water molecule coordinated to Mg2 has also been found by Allen et al.[24] in the structure of XyI with a transition state analog.

Overall, the simulation results support a breathing motion of the magnesium ions accompanying the catalytic cycle of XyI, which is consistent with the mechanism proposed by Whitlow et al.[5] However, Allen et al.,[24] based on the structure of a TS analog, together with the native and the D-glucose complex,[7,8] proposed a slightly different mechanism: after the proton transfer step, as Mg2 moves towards Mg1, it loses three protein ligands (two from the anionic Asp254 and one from the neutral Asp256) while forming only two new coordinations with the sugar. Lavie et al.[8] proposed that a water molecule moves in to fill the remaining coordination

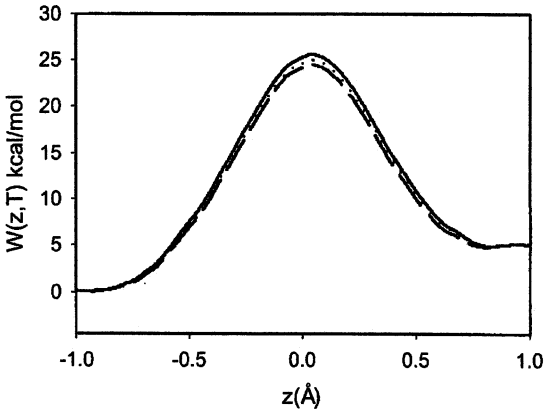

Figure 9. Classical mechanical potential of mean force (solid curve) for hydride transfer and quasiclassical potentials of mean force that include quantum mechanical vibrational free energies for hydride (dashed curve) and deuteride (dotted curve) transfer reactions catalyzed by the xylose isomerase.

site, as seen in the structure of XyI with the transition state analog.[24] However, it is not clear if sufficient binding energy is available to swap an anionic ligand for a neutral water molecule in the first Mg coordination shell.

The metal ion breathing movement observed in our simulation is also consistent with the elliptical shape of the Mg2 electron density in the glucose-complex structure. In the latter case, it is probably the result of a mixture between the reactant state (prior to the proton transfer) and the product state. Mg2 is at position 1 for both enzyme configurations, but the slow movement of the cations, in comparison to the other lighter atoms, allows the detection of Mg2 second position. Position 2 for Mg2 is occupied for a short time, probably comparable to the reaction time scale.

Other Interactions in the Active Center

The average distances between the Mg^{2+} ions and their ligands in the active center of XyI are shown in Table 2, where they are compared with the experimental values. Both Mg^{2+} ions have distorted octahedral coordination. In general the calculated distances are shorter than the experimental ones by 0.3 Å, but they are within the experimental uncertainty range. In addition, Table 2 shows two interactions between protein residues and the substrate that have been proposed to play an important role in the catalytic cycle of XyI. In particular, His53 is involved in the binding of cyclic α-D-xylose and has been proposed to be the catalytic base in the ring-opening step, by shuffling a proton between the O1 hydroxyl and the ring oxygen (O5) of α-D-xylose.[1,5] The crystallographic studies indicate that after this step, the O5 oxygen of D-xylose in extended form is hydrogen bonded to the NE2 atom of His53 in the active center of XyI.[5] This interaction is also found in our theoretical structures (Table 2). On the other hand, the strongest interaction between Lys182 and the O1 atom of the substrate is found in the transition state structure (Table 2), suggesting that this residue contributes to lowering the free energy of activation, as has been proposed experimentally[1] and theoretically.[25]

Table 6. Average Transmission Coefficients for the Hydride Transfer Reaction Using the Static Secondary Zone Approximation at 298 K.

Isotope	Γ	κ	γ
H	0.95	6.91	6.57
D	0.95	3.32	3.16

Primary KIE of the Hydride Transfer Reaction

Figure 9 compares the quasiclassical free energy profiles for the hydride transfer and the deuteride transfer reactions. The inclusion of quantum mechanical vibrational free energy lowers the free energy of activation to 24.1 and 23.7 kcal/mol for the deuteride and hydride transfer reactions, respectively, which gives a KIE of 1.80. In neither case is there a displacement from the classical transition state location due to the inclusion of quantized vibrations in the vibrational free energy. The quasiclassical transition state corresponds to the value $z^* = 0.045$ Å for both isotopes.

We used five minimum energy paths, chosen within the range $z^* = 0.045 \pm 0.06$ Å, to calculate the transmission coefficient. The first column in Table 6 shows the averaged quasiclassical transmission coefficient, which turns out to be the same for both isotopes. Consequently, the correction for classical recrossing does not change the QC KIE value. However, as shown in the second column of Table 6, the introduction of quantum effects on the reaction coordinate increases the KIE by a factor of 2.08, raising the final KIE to 3.75, in good agreement with the experimentally determined KIE at higher temperature. This result clearly demonstrates the importance of including nuclear quantum mechanical effects to reproduce the experimentally determined KIE for light atom transfer reactions. Test calculations with the larger QM system (model 1), for a single reaction path from one configuration in the transition state bin of the CM PMF, give a higher primary KIE as shown in Table 7. The tunneling contribution to the primary KIE is mainly responsible for the different results obtained with the two QM models. Tunneling calculations depend on both the height and shape of the potential of mean force. Although the barriers are essentially the same for the two models, the

Table 7. Computed Primary Kinetic Isotope Effects for the Hydride Transfer Reaction in Xylose Isomerase at 298 K.

	Quasiclassical contribution	Tunneling contribution	KIE
19 QM atoms	1.80[a]	2.08	3.75[b]
79 QM atoms	1.93[a]	2.62	5.01[b]
Experiment			2.7–4.0[c]

[a]From $k^{EA\text{-}VTST}$.
[b]From $k^{EA\text{-}VTST/MT}$.
[c]Refs. 6, 12, 13.

potential surface differs in its detailed shape, causing a change in tunneling contributions. Nevertheless, the results are not markedly different, and they are within the experimental range at higher temperatures, which can be taken as an approximate lower bound on the result at 298 K.

The optimization criterion for choosing the tunneling paths is to choose the larger of the SCT and LCT ones.[36] We found that the SCT transmission coefficient[22] is larger than the LCT one,[37] and so the results in Table 7 are based on the SCT values. In order to determine whether the LCT result might have been unphysically decreased by the SVB term being too large in the large-curvature tunneling swath, we examined the eigenvectors for three saddle point structures with and without the SVB term. To accomplish this we started at the saddle point structure obtained with the SVB term, we removed the SVB term, and we reoptimized the saddle point and calculated $3N_1 - 6$ new frequencies. Among the structures, the mode that corresponds to the quasi-symmetric A–D stretch (mixed a little with the A–H–D bend) varies only slightly (from 1597, 1572, and 1573 cm^{-1} without SVB to 1590, 1566, and 1573 cm^{-1} with SVB, respectively); this is encouraging because a large increase in this frequency might have signaled an underestimate of large-curvature tunneling. In general, the frequencies obtained without the correction term are very close (less than 30 cm^{-1} of difference) to the frequencies for the saddle point structures with the SVB term. Some of them are almost identical, and the total ZPE differs by 0.35–0.37 kcal/mol.

Concluding Remarks

XylI catalyzes the interconversion of glucose and fructose (xylose and xylulose under physiological conditions) and is one of the most widely used enzymes in industry. It has also been investigated by various theoretical techniques.[3,11,18,23,25,49] An important aspect of the active site of XylI is the involvement of two metal-ion cofactors (Mg^{2+} ions) bridged by Glu216.[5,8] X-ray crystal structures showed that the movements of the Mg^{2+} ions are intimately involved in the enzyme-catalyzed reaction.[8,24]

In our study, we employed umbrella sampling with two PES models to determine the potential of mean force for the hydride transfer reaction, the mechanism[5] for which is depicted in Figure 3. These models contain the same number of atoms in the simulation system, but differ in the partition between the QM and MM parts. One model treats the electronic structure of all 19 atoms of the substrate xylose (with its O2 deprotonated) in the QM region, whereas in the other model, the Mg ions and the side chains of all their ligands are also included in the QM representation, giving rise to a total of 79 QM atoms. The rate constants were calculated using CVT with vibrations quantized by instantaneous normal mode calculations and with ensemble-averaged SSZ transmission coefficients to account for both recrossing (Γ_i) and tunneling (κ_i) for each of five secondary-zone configuration i. The two models yielded similar free energies of activation, in particular 25.0 kcal/mol classically and 23.7 kcal/mol including quantum mechanical vibrations. The QC ΔG_{act} is 24.2 kcal/mol for deuteride transfer, a difference of 0.4 kcal/mol from the hydride transfer value.

The calculated H^- shift/D^- shift KIE is 3.75, in good agreement with experimental values in the range 2.7–4.0. Our study demonstrated the significance of including multidimensional tunneling contributions in the calculation of primary KIEs, without which the computed KIE was only 1.8.

An important finding of the present study is the correlation of dynamic fluctuations of the metal ions along the hydride transfer reaction coordinate. Based on the mechanism proposed previously, the two Mg^{2+} take a greater separation in the acyclic xylose complex structure, in which the O2 hydroxy group is neutral and protonated. As the proton of the O2 hydroxy group is abstracted by a hydroxide ligand of the Mg2 ion, resulting in the reactant state for the hydride transfer step, the two magnesium ions have their distance reduced by about 1 Å. Molecular dynamics simulations reveal that the Mg–Mg distance is elongated again accompanying the hydride transfer reaction. This metal ion breathing motion is consistent with the X-ray structures complexed with the reactant glucose and a transition state analogue.

Although the model used in the present calculation has been refined to roughly match the experimental k_{cat} values, our computational results are predictive in several aspects. The computations of the deuterium KIE and tunneling contributions are not related to the parameterization, but the good agreement with the experimental KIE validates the model for transition structure modeling in enzyme reactions. The finding of dynamic motions of the Mg ions coupled to the reaction coordinate is not influenced by the k_{cat} parameterization. Furthermore, the model would still be predictive if one is interested in studying the effects of amino acid mutations on k_{cat}, on dynamic properties, and on tunneling effects.

Acknowledgments

M. G. gratefully acknowledges a Fulbright/Generalitat de Catalunya fellowship. This work was supported in part by the National Science Foundation under grant no. CHE00-92019 and the National Institutes of Health.

Supporting Information

The structure used as a starting point for simulating the hydride transfer step (see "Model" section) is available in PDB format at http://www.chem.umn.edu/groups/gao/publications/.

References

1. He, X.; Agnihotri, G.; Liu, H.-W. Chem Rev 2000, 100, 4615.
2. Bhosale, S. H.; Rao, M. B.; Deshpande, V. V. Microbiol Rev 1996, 60, 280.
3. Fuxreiter, M.; Farkas, O.; Naray-Szabo, G. Protein Eng 1995, 8, 925.
4. Collyer, C. A.; Henrick, K.; Blow, D. M. J Mol Biol 1989, 212, 211.
5. Whitlow, M.; Howard, A. J.; Finzel, B. C.; Poulos, T. L.; Winborne, E.; Gilliland, G. L. Proteins 1991, 9, 153.
6. (a) van Tilbeurgh, H.; Jenkins, J.; Chiadmi, M.; Janin, J.; Wodak, J. S.; Mrabet, N. T.; Lambeir, A.-M. Biochemistry 1992, 31, 5467; (b) Jenkins, J.; Janin, J.; Ray, F.; Chiadmi, M.; Tilbergh, H.; Lasters, I.; DeMaeyer, M.; Belle, D. V.; Wodak, S. J.; Lauwerays, M.; Staussens, P.; Mrabet, N. T.; Snauwaert, J.; Matthyssens, G.; Lambeir, A.-M. Biochmeistry 1992, 31, 5449.

7. Allen, K. N.; Lavie, A.; Petsko, G. A.; Ringe, D. Biochemistry 1994, 33, 1488.
8. Lavie, A.; Allen, K.-N.; Petsko, G. A.; Ringe, D. Biochemistry 1994, 33, 5469.
9. Rangarajan, M.; Hartley, B. S. Biochem J 1992, 283, 223.
10. Farber, G. K.; Machin, P.; Almo, S. C.; Petsko, G. A.; Hajdu, J. Proc Natl Acad Sci USA 1988, 85, 112.
11. Zheng, Y.-J.; Merz, K. M.; Farber, G. K. Protein Eng 1993, 6, 479.
12. Lee, C.; Bagdasarian, M.; Meng, M.; Ziekus, J. G. J Biol Chem 1990, 265, 19082.
13. van Bastelaere, P. B. M.; Kersters-Hilderson, H. L. M.; Lambeir, A.-M. Biochem J 1995, 307, 135.
14. Field, M. J.; Bash, P. A.; Karplus, M. J. J Comput Chem 1990, 11, 700.
15. Gao, J.; Xia, X. Science 1992, 258, 631.
16. Gao, J. Rev Comput Chem 1995, 7, 119.
17. Gao, J.; Amara, P.; Alhambra, C.; Field, M. J. J Phys Chem 1998, 102, 4714.
18. Nicoll, R. M.; Hindle, S. A.; MacKenzie, G.; Hillier, I. H.; Burton, N. A. Theor Chem Acc 2001, 106, 105.
19. Truhlar, D. G.; Garrett, B. C. Annu Rev Phys Chem 1984, 35, 159.
20. Truhlar, D. G.; Isaacson, A. D.; Garrett, B. C. In Theory of Chemical Reaction Dynamics; Bertran, J., Csizmadia, I. G., Eds.; CRC Press: Boca Raton, 1985; pp 65–137.
21. Tucker, S. C.; Truhlar, D. G. NATO ASI Ser C 1989, 267, 291.
22. Liu, Y.-P.; Lynch, G. C.; Truong, T. N.; Lu, D.-H.; Truhlar, D. G.; Garrett, B. C. J Am Chem Soc 1993, 115, 2408.
23. Ferenczy, G.; Naray-Szabo, G.; Varnai, P. Int J Quant Chem 1999, 75, 215.
24. Allen, K. N.; Lavie, A.; Petsko, G. A.; Ringe, D. Biochemistry 1995, 34, 3742.
25. Hu, H.; Liu, H.; Shi, Y. Proteins 1997, 27, 545.
26. Alhambra, C.; Corchado, J. C.; Sánchez, M. L.; Garcia-Viloca, M.; Gao, J.; Truhlar, D. G. J Phys Chem 2001, 105, 11326.
27. Jorgensen, W. L. Adv Chem Phys 1988, 70, 469.
28. Gao, J. Acc Chem Res 1996, 29, 298.
29. Chuang, Y.-Y.; Cramer, C. J.; Truhlar, D. G. Int J Quantum Chem 1998, 70, 887.
30. Garcia-Viloca, M.; Alhambra, C.; Truhlar, D. G.; Gao, J. J Chem Phys 2001, 114, 9953.
31. Anderson, J. B. Adv Chem Phys 1995, 91, 381.
32. Lauderdale, J. G.; Truhlar, D. G. J Chem Phys 1986, 84, 1843.
33. Gao, J.; Pavelites, J. J. J Am Chem Soc 1992, 114, 1912.
34. Wonchoba, S. E.; Truhlar, D. G. J Chem Phys 1993, 99, 9637.
35. Alhambra, C.; Gao, J.; Corchado, J. C.; Villà, J.; Truhlar, D. G. J Am Chem Soc 1999, 121, 2253.
36. Liu, Y.-P.; Lu, D.-h.; Gonzalez-Lafont, A.; Truhlar, D. G.; Garrett, B. C. J Am Chem Soc 1993, 115, 7806.
37. Fernandez-Ramos, A.; Truhlar, D. G. J Chem Phys 2001, 114, 1491.
38. Truhlar, D. G.; Gao, J.; Alhambra, C.; Garcia-Viloca, M.; Corchado, J.; Sanchez, M. L.; Villà, J. Acc Chem Res 2002, 35, 341.
39. Gao, J.; Truhlar, D. G. Annu Rev Phys Chem 2002, 53, 467.
40. Alhambra, C.; Corchado, J. C.; Sánchez, M. L.; Gao, J.; Truhlar, D. G. J Am Chem Soc 2000, 122, 8197.
41. Amara, P.; Field, M. J.; Alhambra, C.; Gao, J. Theor Chem Acc 2000, 104, 336.
42. Devi-Kesavan, L. S.; Garcia-Viloca, M.; Gao, J. Theor Chem Acc, to appear.
43. Case, D.; Kattalam, J. J Am Chem Soc 1998, 100, 7690.
44. (a) Brooks III, C. L.; Karplus, M. J Chem Phys 1983, 79, 6312; (b) Brooks III, C. L.; Karplus, M. J Mol Biol 1989, 208, 159; (c) Alhambra, C.; Gao, J. J Comp Chem 2000, 21, 1192.
45. Brooks, B. R.; Bruccoleri, R. E.; Olafson, B. D.; States, D. J.; Swaminathan, S.; Karplus, M. J Comput Chem 1983, 4, 187.
46. Stewart, J. J. P. J Comput Chem 1989, 10, 209.
47. Mackerell, A. D.; Bashford Jr, D.; Bellott, M.; Dunbrack, R. L.; Evanseck, J. D.; Field, M. J.; Fischer, S.; Gao, J.; Guo, H.; Ha, S.; Joseph-McCarthy, D.; Kuchnir, L.; Kuczera, K.; Lau, F. T. K.; Mattos, C.; Michnick, S.; Ngo, T.; Nguyen, D. T.; Prodhom, B.; Reiher III, W. E.; Roux, B.; Schlenkrich, M.; Smith, J. C.; Stote, R.; Straub, J.; Watanabe, M.; Wiorkiewicz-Kuczera, J.; Yin, D.; Karplus, M. J Phys Chem B 1998, 102, 3586.
48. Jorgensen, W. L.; Chandrasekhar, J.; Madura, J. D.; Impey, R. W.; Klein, M. L. J Chem Phys 1983, 79, 926.
49. Naray-Szabo, G. Comput Chem 2000, 24, 287.
50. Hutter, M. C.; Reimers, J. R.; Hush, N. S. J Phys Chem B 1998, 102, 8080.
51. Gonzalez-Lafont, A.; Truong, T. N.; Truhlar, D. G. J Phys Chem 1991, 95, 4618.
52. Alhambra, C.; Corchado, J. C.; Villa, J.; Gao, J.; Truhlar, D. G. CHARMMRATE, version 1.0; a module of CHARMM, version 27; University of Minnesota: Minneapolis, MN, 2000.
53. Corchado, J. C.; Chuang, Y.-Y.; Fast, P. L.; Vill, J.; Hu, W.-P.; Liu, Y.-P.; Lynch, G. C.; Nguyen, K. A.; Jackels, C. F.; Melissas, V. S.; Lynch, B.; Rossi, I.; Coitio, E. L.; Steckler, R.; Garrett, B. C.; Isaacson, A. D.; Truhlar, D. G. POLYRATE, 8.5b; University of Minnesota: Minneapolis, MN, 1999.
54. Press, W. H.; Flannery, B. P.; Teukolsky, S. A.; Vetterling, W. T. Numerical Recipies; Cambridge University Press: Cambridge, 1986; 412.
55. Garrett, B. C.; Redmon, M. J.; Steckler, R.; Truhlar, D. G.; Baldridge, K. K.; Bartol, D.; Schmidt, M. W.; Gordon, M. S. J Phys Chem 1988, 92, 1476.
56. Møller, C.; Plesset, M. S. Phys Rev 1934, 46, 618.
57. Hehre, W. J.; Radom, L.; Schleyer, P. V. R.; Pople, J. A. Ab initio molecular orbital theory; Wiley: New York, 1986.
58. Gao, J. MCQUM 3.0, Monte Carlo QM-MM; University of Minnesota: Minneapolis, MN, 2000.